The following publication Y. Wang, Y. Wang, I. W. -H. Ho, W. Sheng and L. Chen, "Pavement Marking Incorporated With Binary Code for Accurate Localization of Autonomous Vehicles," in IEEE Transactions on Intelligent Transportation Systems, vol. 23, no. 11, pp. 22290-22300, Nov. 2022, is available at ttps://dx.doi.org/10.1109/TITS.2022.3173656

Pavement Marking Incorporated with Binary Code for Accurate Localization of Autonomous Vehicles

Yuhao Wang, Yuhong Wang, Ivan Wang-Hei Ho, *Senior Member, IEEE*, Wei Sheng, Ling Chen

***Abstract*—Accurate localization is a critically important issue for autonomous vehicles as it is closely related to the safety and efficiency of autonomous driving. However, current technologies for autonomous vehicle localization face many challenges. To provide accurate and robust localization services to autonomous vehicles, we propose a novel solution by employing a newly designed pavement marking. This marking operates on color contrast, temperature contrast, and binary code with some special features. We also trained and customized an object detector based on a deep learning model: YOLOv5, and integrated it with the decoding algorithm. The localization system is capable of running at a steady frame rate of more than 50 FPS. Road trials up to 80 km/h were conducted, and satisfactory results confirmed the feasibility and robustness of the localization system. Specifically, with a common onboard camera, more than four continuous frames can be detected and decoded correctly when the speed is slower than 30 km/h. At least one frame can be detected and decoded correctly at a higher speed (i.e., 30 – 50 km/h). With a high-speed camera, more than 18 frames can be detected and decoded even at 80 km/h. The findings suggest that the specially designed road marking and associated algorithms can provide a viable and economical option for accurate localization of autonomous vehicles. The performance of the system has potentials for further improvement by using better hardware such as faster CPUs, GPUs, and thermal imaging techniques.**

***Index Terms*—Accurate Localization, Pavement Marking, Object Detection, Binary Code.**

I. Introduction

ACCURATE vehicle localization based on modern techniques has received much attention, but the potential capabilities of pavement markings are often ignored because researchers are much attracted by roadside infrastructures. After the first autonomous vehicle was introduced by Google Inc. in 2009, there was an upsurge in the development of autonomous vehicles in the following decade [1]. Jo [2] concluded that five functions are essential for autonomous vehicles: Localization, perception, control, planning, and system management. An accurate and robust localization function is fundamental to all other functions [3], and centimeter-level accuracy is required to realize level four and above vehicle autonomy.

Conventional global positioning system (GPS) technique usually suffers blockage, multipath propagation, and None Line-of-Sight (NLOS) problems and merely warrants the accuracy of 7-13 meters in an open area [4]. Generally, severe signal deterioration happens in an urban area with high-rise buildings, under elevated freeways, and in indoor parking structures or tunnels. Existing literature on improving GPS accuracy is extensive and mostly focuses on data fusion and system integration. For example, two typical GPS and WiFi integrated systems were proposed in [5] and [6]. The first system matches the GPS data with the local map data distributed by roadside units (RSU) through WiFi, and the second system takes advantage of the signal strength characteristics of WiFi and utilizes a Kalman filter to estimate the precise location. Overall, relevant studies leverage the power of WiFi either by delivering the data to vehicles through WiFi [5] or by utilizing its own characteristics as fingerprint such as received signal strength [6], [7], and channel state information [8] to perform localization. An early example of research into GPS data fusion is [9] in which the Kalman filter was utilized to fuse the high definition map data, GPS data, and camera data to localize the vehicle. This technique highly depends on the map data which means it is impractical when a map database lacks. To address this challenge, LIDAR was proposed for either the environment perception in [10] or road marking detection in [11] to assist the vehicle localization. In addition to these types of data, another study utilized the sensor data (i.e., inertial sensor data, speedometer data, and vision sensor data) to estimate the lateral position [12].

Extensive research has shown that autonomous vehicle localization assisted with roadside WiFi can achieve accuracy less than 2 meters [13]. However, continuously evolving vehicular technology and increasing traffic demand pose tremendous challenges to the development of roadside infrastructures. The spatial and physical constraints caused by intensive urban development cannot support the rapid proliferation of roadside infrastructures in urban areas. Moreover, public concerns about visual impact, environmental issues, tax burden and impacts on existing traffic, etc., make it rather challenging to build new roadside infrastructures [14]. These barriers might prevent autonomous vehicles from accessing accurate localization services provided by introducing new roadside infrastructures in the urban area.

Accurate localization aided by pavement marking is an alternative way to overcome these barriers. In contrast to the roadside facilities, there are no spatial constraints when introducing a new marking onto road pavement surface, especially in overcrowded urban areas. Pavement markings are necessary components for road infrastructures with large impacts on travel safety [15]. They offer directions, give

Y. Wang and I. W.-H. Ho are with the Department of Electronic and Information Engineering, The Hong Kong Polytechnic University, Hong Kong (e-mail: yuhao1995.wang@connect.polyu.hk, ivanwh.ho@polyu.edu.hk).

W. Sheng, Y. Wang and L. Chen are with the Department of Civil and Environmental Engineering, The Hong Kong Polytechnic University, Hong Kong (e-mail: yuhong.wang@polyu.edu.hk)

Manuscript received April 19, 2005; revised August 26, 2015.

warnings, and provide information to drivers. For example, it was proved in [16] and [17] that markings can effectively reduce speeds before the upcoming hazard and thus prevent accidents. Recent advances in deep-learning-based computer vision techniques have enabled autonomous vehicles to detect and localize road markings reliably. [18] proposed to employ a binarized normed gradient method to detect road markings and utilize a principal component analysis network to classify up to nine classes of road markings. [19] focused on the detection and classification of arrows and bike marking using an integration methodology based on an adaptive region of interest and deep convolutional neural network. To jointly handle lane and road marking detection and recognition, [20] proposed a vanishing point guided network and built a dataset to address the shortcoming of lacking a benchmark dataset. Furthermore, reducing detection complexity and maintaining high accuracy at the same time in the detection is critically important. [21] developed a deep convolutional neural network to extract robust lane marking features and further designed a shallower and thinner structure to reduce the computation burden. [22] modified the VGG-16 base network to boost the overall detection performance.

There are relatively few studies in the area of accurate localization with pavement marking. In [23], the researchers fused the GPS data, sensor data, and road marking position to localize vehicle lateral distance. Similarly, [12] integrated the GPS and road marking detection for vehicle localization. Another study proposed to deduce the absolute global location information based on a preliminary survey of road making locations and relative real-time road marking features captured by onboard cameras [24]. Road-SLAM was introduced in [25], and this study employed a random forest algorithm to match the map with the road marking pictures captured by onboard cameras. However, taken together, these studies are costly in the preliminary survey for database development, and they highly rely on the presence of road markings. Except near the intersections, road markings are distributed sparsely, and they are usually highly repetitive, making them hard to distinguish with the proposed methodology.

Adding information to the existing pavement lane markings is also a feasible way to help localize the vehicles. [26] painted pavement lane line markings with yellow color to code the markings. That helped localize the vehicles coarsely and realized metric localization by matching visual points around the marking area. Nevertheless, it is difficult to distinguish the painted markings in a complicated environment because they paint the markings in a simple color, and the method is only effective within a small range. It cannot provide absolute global location information.

Basic road markings are not limited by spatial constraints and have no electronic elements, which guarantees a secure operational state. Additionally, recent advances in computer vision technique and artificial intelligence (AI) enable autonomous vehicles to sense road markings more accurately [27]. Nevertheless, accurate localization techniques still need to be further improved to guarantee the safety and reliability for the next-generation vehicle. To address the challenges mentioned above, this paper attempts to extend the potential capabilities of road marking-aided localization and achieve the following objectives.

- We propose a novel road marking methodology based on color contrast, temperature contrast, and binary coding principle to provide autonomous vehicles with accurate and robust localization services.
- We encode the absolute global position information into the newly designed road pavement marking, which can achieve decimeter-level accuracy.
- We train a deep-learning-based object detection tool to detect and crop the marking images captured by onboard cameras. We also propose a corresponding decoding algorithm to decode the cropped images.
- We conduct practical road trials to rigorously evaluate the performance of the proposed novel pavement marking and the corresponding algorithms.

Compared with the previous methodologies, the following advantages are achieved:

- Introduce a novel marking to the pavement to provide reliable absolute global location information with decimeter-level accuracy.
- Provide redundant localization service to meet the safety and robustness requirements of autonomous vehicles and V2X operations.
- Provide reliable, robust, and flexible services in challenging road environments (e.g., foggy conditions and low illumination conditions).
- Enable easy and efficient detection thanks to two-dimensional coding with strong anti-interference capability.
- Address spatial, physical, and financial constraints because roadside facilities are not needed, and the costs of the road markings are very low.

The rest of this paper is organized as follows. Section II introduces the workflow of the localization system, the technical details of the newly designed pavement marking, and the algorithm of marking detection and decoding; Section III deals with the road trial configurations and results, and Section IV concludes the paper.

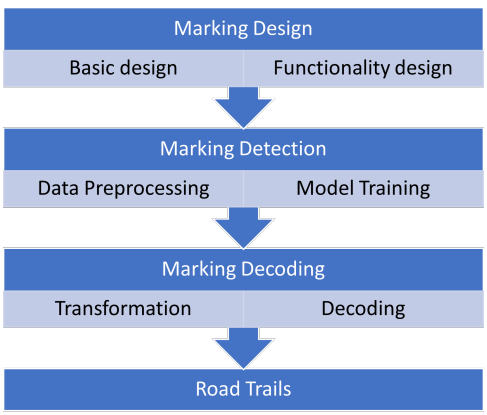

Fig. 1. The overall structure of this study.

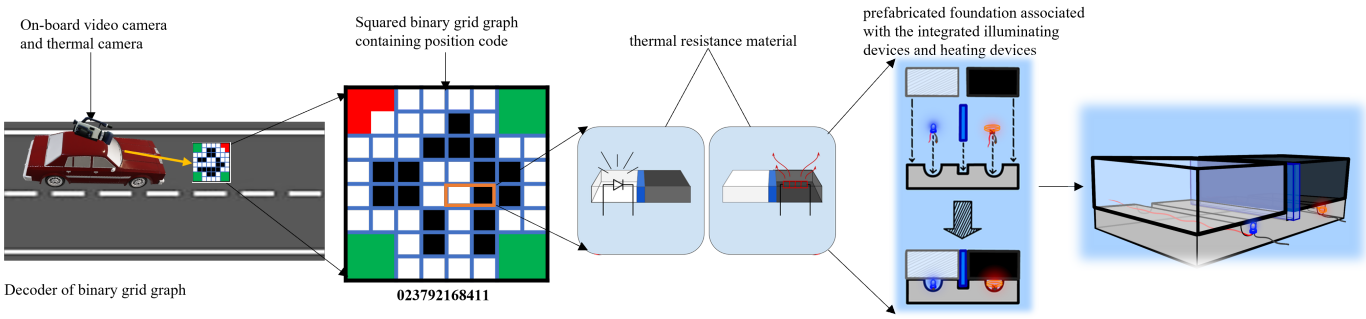

Fig. 2. The technical details and the overall operating principles of the novel road pavement marking.

II. Proposed Methodology

A. Problem Analysis

Motivated and inspired by existing studies, this paper aims to develop a newly designed pavement marking to provide accurate and robust localization services to autonomous vehicles, especially in cases where GPS and roadside infrastructure localization methodology cannot work. As shown in Fig. 1, the overall framework of this study consists of four stages. The framework commences with marking design. The technical details of the novel marking are introduced here, including essential elements, operating principles, and functionality design. The next stage is marking detection, where the data preprocessing and the model training of the deep-learning-based marking detector are presented. The following stage is marking decoding which explains how to precisely crop and transform the marking image to decode the location information. Finally, road trials are conducted, and the results are analyzed in detail.

B. Novel Road Marking for Accurate Localization

The novel road pavement marking can provide accurate (i.e., lane-level) absolute global location services to autonomous vehicles with reliability and robustness due to its high color contrast ratio, thermal difference, and flexible graphical variations. In principle, the novel road localization marking is made of the following components:

- Squared binary grid-shaped objects with different graphic patterns, temperature contrast, and color contrast are utilized to express the ten numbers of 0-9.
- These grid-shaped objects are arranged according to the absolute global location coordinates to form a bigger grid-shaped graphic pattern number matrix.
- Thermal insulation material is employed here to isolate each grid unit.
- The pattern matrix is complemented by positioning detection markers located on the three corners of the matrix (i.e., boundary markers).
- All the components are integrated on a prefabricated base plate for industrial production and installation on the pavement.
- Heaters and illumination devices are integrated on the base plate to enhance the luminosity contrast ratios and temperature differences (optional); One may also use reflective coating for such purpose.

1) Operating Principle: The overall operating principle is shown in Fig. 2. This marking is embedded in the specific position of the road pavement, usually in the middle of a traffic lane to avoid vehicle-caused wear and tear. The marking is embedded in the pavement and covered with a piece of translucent layer to withstand the traffic loads and long-term environmental impacts. The translucent layer requires adequate structural performance (e.g., durability, fatigue resistance, and stiffness) and functional requirements (sliding resistance and water resistance) to guarantee traffic safety and protect the electronic elements. Usually, inorganic and high molecular polymers are employed, such as toughened glass and polymethyl methacrylate. Previous works have already applied these materials on the surface of solar pavements, and they are well-reviewed in [28]. The absolute global location is encoded in the marking. In the cases of poor illumination conditions and foggy environment, the marking can turn on the heaters and illumination devices automatically. When a vehicle passes by, the marking is captured by the visual cameras and thermal cameras installed on the vehicle. Then, the exact location of the vehicle is calculated according to the decoded marking, captured marking size, azimuth angle, and elevation angle.

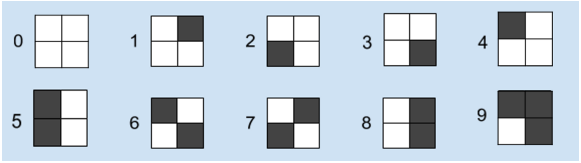

Fig. 3. An encoder based on color contrast.

2) Binary code and its boundary markers: The binary grid-shaped objects are employed to express the ten numbers 0-9. Each grid-shaped object represents a number called the ”basic cell”. Each basic cell contains four ”basic units”. The unit contains objects with different patterns, and the difference between basic units expresses 0 and 1 of the binary code. Since four basic units are contained in each basic cell, the capabilities of a basic cell can be extended to represent a hexadecimal digit. Generally, the size of the basic unit is 2-5 centimeters. The units are separated by thermal insulation material and the thickness is 0.2 centimeters to 1 centimeter. The marking is encoded from left to right, from top to bottom. The last one or two binary code can be used as error correction code if needed. The preliminary idea is to set the error

correction code to the last one or two digits of the sum of the geographical information codes. An example of an encoder based on color difference is shown in Fig. 3. Although this example utilizes black and white to achieve color differences, other groups of different colors can also play the same role. In addition, other shapes (e.g., circles and triangles) besides squares can also be employed.

Illumination conditions, weathers, pavement debris, and air pollution affect the color difference. To ensure the safety of autonomous vehicles, adequate redundancy and reliability must be ensured. We intend to enhance them by adding the following features:

i **Basic unit with enhanced color difference:** The basic units of the basic cell consist of wear-resistant glass, concrete, polymer, and other material and these materials are made with different colors. The color contrast can be enhanced by adding toner. The performance of the unit at night or in poor illumination conditions can also be improved by adding reflective glass micro-beads, phosphors, and other materials during production.

ii **Basic unit with thermal absorption and conductivity difference:** The basic units of the basic cell are different in thermal absorption, thermal conductivity, and other characteristics due to differences in materials and colors, leading to the differences in surface temperature. After the thermal image is captured by the onboard thermal camera, we can decode the absolute global location.

iii **Basic unit with graphic pattern difference:** The basic units of the base cell differ in graphic patterns (optional). The differences in graphic patterns can be used together with (i) and (ii) features to further enhance the redundancy and error correction of image processing. Fig. 4. gives an example of the 4 basic units of a base cell containing the differences both in color and graphic patterns.

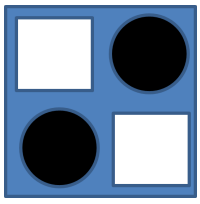

Fig. 4. Four basic units of a basic cell containing differences both in color and graphic patterns.

In order to facilitate the identification of the boundary of the road marking and minimize the disturbance in computer post-processing, there are four boundary markers around it (i.e., three of them are the same, and the other one represents the starting point of the decoding region). The boundary markers allow the computer to accurately recognize the marking and read it at high speed while indicating the direction in which the marking is presented. They help quickly identify the presence of the marking in an image and its orientation. An example is given in Fig. 5., where the red triangles represent the starting point of decoding, and the three squares are the corners of the decoding region. The preferred scheme is triangles and rectangles with obvious boundaries, but other shapes can play the same roles as well.

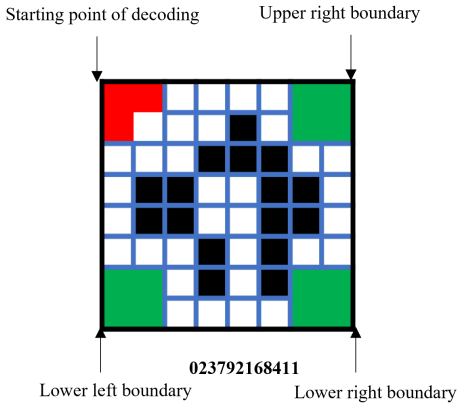

Fig. 5. Boundary markers of an example marking.

3) Heaters and illumination devices (optional): Changes in the intensity of illumination and temperature conditions lead to the reduction of the contrast ratio, thereby affecting the accuracy of the marking detection and traffic safety. We propose to integrate the heaters and illumination devices on the base plate as an aid to enhance the luminosity contrast ratios and temperature differences so as to help the marking detection in a challenging road use environment. As shown in Fig. 2, the semi-transparent material is used for the light-colored basic unit cover while the dark-colored basic unit has no such requirement. Furthermore, thermal insulation material different from these two colors is employed here to isolate each unit of the grid. Its main functionality is to reduce the heat conduction between different color basic units and thus increase the temperature difference. The secondary function is to distinguish the boundary between each unit. Generally, the illumination device (e.g., LED) is installed under the light-colored unit, and the heater is installed under the dark-colored unit. The illumination devices and heaters can be integrated under the boundary markers as well.

As shown in Fig. 2, all the basic cells and devices are integrated on a prefabricated solid base plate for industrial production and installation on the pavement. The base plate can be made of metal or concrete. Grooves are preset on the surface of the base plate. The heaters, illumination devices, and wires are installed in the grooves to protect the devices from being compressed. Cold light sources (e.g., LED) are preferred to guarantee the thermal differences. The installation process of a basic cell is demonstrated in the rightmost figure of Fig. 2. Firstly, the devices and wires are placed in the grooves of the base-plate. After that, the basic unit is installed on the base plate with glue. The dimensions of the plate are 15 centimeters to 50 centimeters in length, 15 centimeters to 50 centimeters in width, 0.5 centimeters to 5 centimeters in thickness.

C. Marking Detection based on YOLOv5

We employ an object detection algorithm to enable the onboard computer to ”detect and recognize” the newly designed marking. Historically, the sliding window-based region

selection strategy was utilized in object detection research [29]. However, this method is complex and not targeted, leading to low efficiency. Thanks to the rapid development of computational power and artificial intelligence in recent years, deep learning methodology, especially convolutional neural network (CNN), has been used in object detection. A major advantage of CNN is that there is no need to design the feature extractors manually [30]. You Only Look Once (YOLO) is an object detection algorithm that was firstly proposed by Redmon in 2016 [31]. The most advanced version up to now is YOLOv5 based on Pytorch, which was developed by Jocher et al. in 2020 [32]. It is one of the most well-known one-stage object detection algorithms due to its speed and accuracy. YOLOv5 firstly segments the image into a grid system and then detects the object in each cell. YOLOv5 is divided into three segments: Backbone CSPDarknet, Neck PANet, and head YOLO Layer. The input image size is $640 \times 640 \times 3$, and then the image flows through the backbone, becoming a $320 \times 320 \times 12$ feature map. In the Neck part, the information flow is boosted, and the newly adopted feature pyramid network enhances the spreading of the low-level features. In the last YOLO layer, three different sizes of feature maps are generated to adapt to different size targets that fit the marking detection scenario because the onboard camera usually sees the marking from far to near, from small to large. The output size is five times the category size (i.e., x, y, height, and width of the prediction box and confidence). The whole structure of YOLOv5 can be referred to [33]. Compared with EfficientDet, all YOLOv5 models run better (i.e., larger COCO AP) and faster (i.e., less GPU processing time) on COCO dataset [32]. Compared with the previous version, such as YOLOv3 and YOLOv4, YOLOv5 outperforms others in terms of accuracy of detection [34].

In this paper, we utilize YOLOv5s (i.e., the most basic one of the four official YOLOv5 models) to train our custom data because high speed and small size are needed to embed the program in autonomous vehicles. Firstly, we collect the data set and then use the data for both training and validation. Then we create a label for each piece of data and modify the default classifier to one, which is the novel marking. Lastly, we train the data and generate the weights of the model. The model is exported to our local system for further road trials.

Algorithm 1: Marking Decoding

input : Cropped Image $\mathbf{X}$ with a size of $x_c \times x_r$ from YOLOv5

output: A number sequence containing absolute global position

Initialize the threshold values: α°_{red} , α°_{green}, β, γ *and* ε;
Convert $\mathbf{X}$ to HSV image $\mathbf{x}$;
$\mathbf{x} = [\mathbf{p}_{m,n}]_{x_c \times x_r}$, $\{h_{\mathbf{p}_{m,n}}, s_{\mathbf{p}_{m,n}}, v_{\mathbf{p}_{m,n}}\} = \mathbf{p}_{m,n}$;
for $i \leftarrow 1$ **to** x_r **do**
  for $j \leftarrow 1$ **to** x_c **do**
    if $\{h_{\mathbf{p}_{i,j}}, s_{\mathbf{p}_{i,j}}, v_{\mathbf{p}_{i,j}}\}$ *yeilds Equation (1)* **then**
      $\mathbb{G}_{i,j} = 1$
    else
      $\mathbb{G}_{i,j} = 0$
for $i \leftarrow 1$ **to** x_r **do**
  for $j \leftarrow 1$ **to** x_c **do**
    if $\{h_{\mathbf{p}_{i,j}}, s_{\mathbf{p}_{i,j}}, v_{\mathbf{p}_{i,j}}\}$ *yeilds Equation (2)* **then**
      $\mathbb{R}_{i,j} = 1$
    else
      $\mathbb{R}_{i,j} = 0$
Find top 3 largest open area in $\mathbb{G}$ and top 1 largest open area in $\mathbb{R}$ and denoted by $\mathbb{G}'$ and $\mathbb{R}'$;
$\mathbf{x}_1 = \{\mathbb{G}', \mathbb{R}'\}$;
Find the corners $\mathbb{V}_{candidate}$ of $\mathbf{x}_1$ Find four vertices of the marking $\mathbb{V}$ according to the Equation (3);
Geometric transformation of $\mathbf{X}$ from $\mathbb{V}$ to $\mathbb{V}_{sqare}$ projectively and get image $\mathbf{x}_2$;
Gird the marking and get $\mathbf{x_3} = \{x_i, \forall i \in \mathbb{N}_{\leq 64}\}$;
foreach *unit* x_i*in* $\mathbf{x_3}$ *grid* **do**
  Calculate the average pixel value of each unit a_i; **if** $(a)i \geq \varepsilon$ **then**
    The basic unit x_i is white, $\mathbb{M}_i = 1$
  else
    The basic unit x_i is black, $\mathbb{M}_i = 0$
Based on $\mathbb{M}$ and encoder, decode the marking and output the number sequence;

D. Marking decoding algorithm

After marking detection, the video frame containing the novel marking is extracted and cropped according to the prediction box's coordinates, height, and width. Once the marking is extracted, the cropped image is exported to the marking decoding algorithm based on Matlab. This is achieved by calling Matlab API (i.e., Matlab Engine) from python, and the API is integrated into the main script of YOLOv5. The proposed marking decoding algorithm is based on the CV tool embedded in Matlab. The overall workflow of the decoding algorithm is shown in Fig. 6 and Algorithm 1 and explained as follows.

1) Detect the boundary markers: The frame is cropped by YOLOv5 so that only the desired part containing the marking remains. However, the cropped image still contains futile pixels. That is because the YOLOv5 algorithm only produces quadrilateral images, while the marking on the road captured by the camera is not in that shape due to the elevation and azimuth angle of the onboard camera. Thus, boundary detection and image transformation are necessary to decode the marking. This step can help increase the accuracy of decoding significantly. Take the red and green boundary markers as an example to introduce the boundary marker detection algorithm. In this example, there are three square green boundary markers and one triangle red boundary marker representing the starting point of the decoding. HSV (i.e., hue,

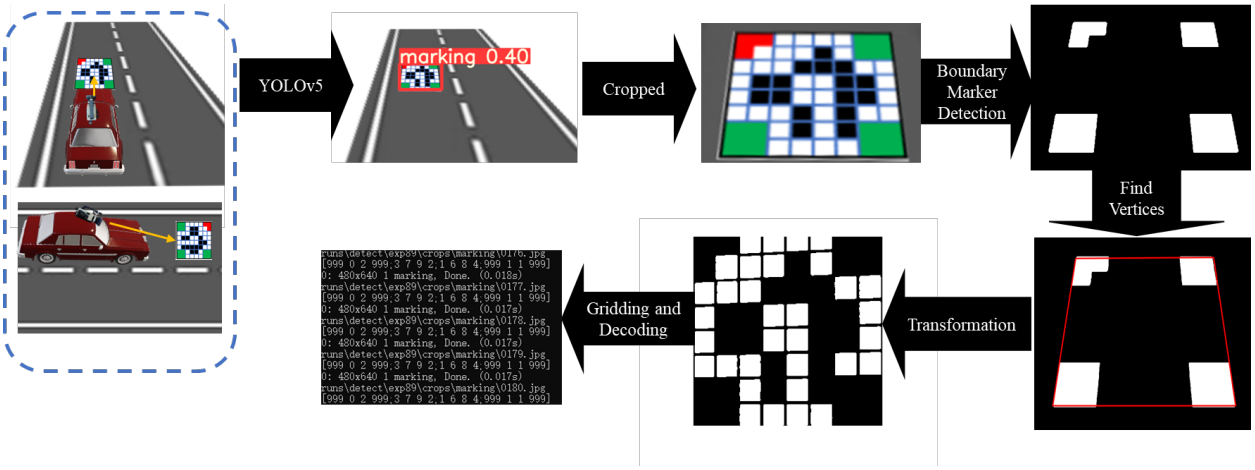

Fig. 6. The flowchart of the marking detection and decoding.

saturation, and value) is an alternative representation of color other than RGB (i.e., red, green, and blue) and it is more closely aligned with the way human vision perceives color. HSV is used here to recognize the color of boundary markers because the road environment is changing all the time, and this leads to the brightness and saturation changes of the boundary markers. HSV can recognize red and green effectively.

Let $\mathbf{X}$ denote the cropped image. $\mathbf{X}$ is a three-dimension matrix with a shape of $x_c \times x_r \times 3$. The first two dimensions are the width and height of the image denoted by x_c and x_r. The third dimension is the RGB value of each pixel. After converting $\mathbf{X}$ to an HSV image, the shape of the new $\mathbf{x}$ will not change but the third dimension represents the HSV value. $\mathbf{x}$ is the input of the decoding algorithm. Let $\{h_{\mathbf{p}_{m,n}}, s_{\mathbf{p}_{m,n}}, v_{\mathbf{p}_{m,n}}\} = \mathbf{p}_{m,n}$ denote the HSV value list of pixel $\mathbf{p}_{m,n}$ which is within the image $\mathbf{x} = [\mathbf{p}_{m,n}]_{x_c \times x_r}$ and locates in the mth row and nth column, where $m \leq x_r$ and $n \leq x_c$. To detect a specific color that contains different saturation and brightness, we need to set the threshold value of HSV. Specifically, the true red color locates in $h = 0°, \forall s, v$ and true green is $h = 120°, \forall s, v$in HSV. The range of the threshold value of h of red color is set to α°_{red} and green color h is set to α°_{green}. The minimum threshold values of s and v are both set to β and γ. Then, in our assumed scenario, all the green pixels of the boundary markers are in the set $\mathbf{p}_{m,n} \in \mathbb{G}$ where

$$120° - \frac{\alpha^{\circ}_{green}}{2} \leq h_{\mathbf{p}} \leq 120° + \frac{\alpha^{\circ}_{green}}{2}, \forall s_{\mathbf{p}} \geq \beta, \forall v_{\mathbf{p}} \geq \gamma \tag{1}$$

The set of red marker pixels $\mathbf{p}_{m,n} \in \mathbb{R}$ is defined as

$$0° - \frac{\alpha^{\circ}_{red}}{2} \leq h_{\mathbf{p}} \leq 0° + \frac{\alpha^{\circ}_{red}}{2}, \forall s_{\mathbf{p}} \geq \beta, \forall v_{\mathbf{p}} \geq \gamma. \tag{2}$$

After collecting the data sets, we convert the image to a binary image (i.e., set red pixels to 0 and the others to 1) to reduce the burden of computation. Then we find all the open areas of the binary image and eliminate the smaller ones except for the largest one which is the red boundary marker. This is because the YOLOv5 algorithm has already excluded the other red pixels. Let $\mathbb{R}'$ denote the new red pixel set. Finding the three green boundary markers is based on the same principle and we only need to keep the top-three open areas. Let $\mathbb{G}'$ denote the new green pixel set. Last, we combine the two types of boundary markers together and get the $\mathbf{x}_1$ where $\mathbf{x}_1 = \{\mathbb{G}', \mathbb{R}'\}$.

2) Find the vertices of the marking: $\mathbf{x}_1$ is the binary image of boundary markers as shown in the second figure in Fig. 6. The white pixels represent the boundary markers. The four vertices of the marking denoted by $\mathbb{V} = \{\mathbf{r}, \mathbf{c}\}$ is defined as the four white pixels in $\mathbf{x}_1$ which are closest to the vertices of the input image $\mathbf{x}$. First we define the four vertices of the image $\mathbf{x}_1$ as a set of target vertex coordinates of $\mathbf{x}$ as $\mathbb{V}_{target} = \{\mathbf{r}', \mathbf{c}'\}$ in which $\mathbf{r}' = [0, 0, x_r, x_r]$ and $\mathbf{c}' = [0, x_c, 0, x_c]$. In the following, we utilize the Harris-Stephens algorithm to detect the corner points denoted by $\mathbb{V}_{candidate} = \{\mathbf{r}'', \mathbf{c}''\}$ as the candidates of the marking vertices. Then, among these candidates, we find the four pixels that are closest to the $\mathbb{V}$ and this can be expressed as:

$$\mathbb{V} = \underset{\{\mathbf{r},\mathbf{c}\}}{\arg\min} \quad \|\mathbb{V}_{target} - \mathbb{V}_{candidate}\|. \tag{3}$$

3) Image transformation: The obtained $\mathbb{V}$ is the set of the vertices of a quadrilateral pattern that contains the marking. However, images with irregular shapes are difficult to be decoded, and it also reduces the accuracy significantly. In this part, we transform the irregular quadrilateral image into a square one. We denote the square-transformed and precisely cropped image as $\mathbf{x}_2$, and the side length of the desired square image is 300 pixels. The new vertices of the desired square marking thus are $\mathbb{V}_{square} = \{\mathbf{r}''', \mathbf{c}'''\}$ in which $\mathbf{r}''' = [0, 0, 300, 300]$ and $\mathbf{c}''' = [0, 300, 0, 300]$. The transformation methodology is projective since the scene appears tilted. Additionally, we want the straight lines to remain straight and recover the original parallel lines that now converge toward a vanishing point. Then we fit the geometric transformation of $\mathbb{V}$ to the control point pairs $\mathbb{V}_{square}$ and get the geometric transformation information. Lastly, we apply the fitted geometric transformation to the image $\mathbf{x}$ and crop the marking image precisely. Now we get the square-transformed

and precisely cropped image $\mathbf{x}_2$ where only the marking presents.

4) Grid the marking and decoding: After the above pre-processing, we obtain a square marking image, and it enables us to decode the marking correctly and efficiently. As shown in Fig. 5, the marking is encoded with 12 digits in the assumed scenario. It has eight basic units on each side and 64 basic units in total. After subtracting the 16 basic units including the boundary markers, 48 basic units need to be counted and 12 basic cells to be decoded. Therefore, we divide the square marking into 64 smaller square images equally. Firstly, we convert the color image to a binary image to reduce the computation burden and ensure that we can conduct the marking decoding algorithm in real-time together with YOLOv5. After that, we divide the marking image into a 8×8 grid denoted by $\mathbf{x} = \{x_i, \forall i \in \mathbb{N}_{\leq 64}\}$. Basically, each grid represents one basic unit. In the binary image, the white pixel is 0, and the black pixel is 1. Consequently, the color of the basic unit can be defined by calculating the average value of all the pixels in x_i. The average pixel value of each basic unit is then compared with the threshold value ε. If the average value is larger than ε, it is a black unit; otherwise, it is white. Finally, based on the encoder proposed in sub-section B, the final digits can be decoded by checking the color of the basic units in each basic cell. However, not all of the detected markings can be correctly decoded. When the marking is far from the camera, it only presents in a few pixels, making it blurry and hard to decode. When the marking is about to leave the viewfinder, only part of the marking can be captured. The incorrect decoding scenarios are fully considered, and all the related algorithms are integrated into the decoding algorithms. The frames that contain the marking in the following scenarios are filtered out by the algorithm:

- Any of the three square green boundary markers cannot be found, or the number of the green open areas is less than three.
- The triangle red boundary marker cannot be found.
- Any of the four vertices cannot be found, or the number of the vertices is less than four.
- The coordinates of the four vertices are beyond the coordinates of the boundary markers.
- The digits cannot be decoded by the decoder due to incorrectly calculated pixel value or wrong code combinations.

III. Road Trials

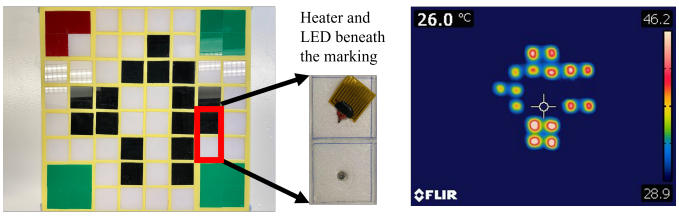

Fig. 7. A demo of the novel marking made in the laboratory and its thermal image after turning on the heaters.

Road trials were carried out to evaluate the performance of the novel road marking made by our research team. As shown in Fig. 7, the marking contained 64 basic units, and each side had eight units. Four boundary markers were made up of 16 basic units located on the four corners. The other 48 basic units were groups of four each and constituted an ordered 12-number sequence. To test the consistency and reliability of the proposed algorithm, we randomly generated the sequence, but we assumed that the sequence carried the absolute global information of the position where the marking was installed. The integer parts of global longitude and latitude cover an enormous area, and they seldom change within a city. They can be obtained from GPS accurately without an error. Thus, there is no need to include it in the marking. In addition, six decimals have already achieved a 0.1-meter accuracy for both longitude and latitude. In the marking sequence, the first six numbers represented the decimal part of the longitude, and the last six numbers represented the decimal part of the latitude. Each basic unit was a square with a side length of 3.5 centimeters. The thermal insulation material was 5 millimeters in thickness. The total side length of the marking was 32.5 centimeters. The basic unit was made of a high-strength acrylic board. LED was embedded under the light-colored unit, and the heater was beneath the dark-colored unit. We used a FLIR thermal camera to test the performance of the heaters, as demonstrated in Fig. 7. All the devices were integrated on a base plate.

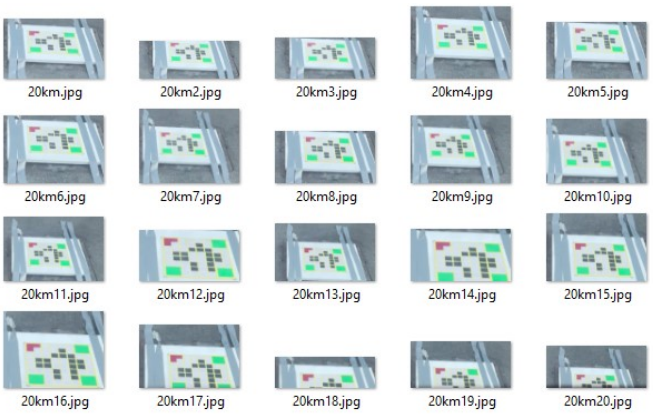

Fig. 8. Examples of images cropped by YOLOv5 at a speed of 20 km/h.

Before conducting the road trials, the deep-learning-based marking detector was trained. Fifty images of the novel road marking demo were captured in different environments. Forty images of them were used to train the model, and ten images were for testing. Then, the decoding algorithm was integrated into the YOLOv5 program and ran in real-time. The frame rate could achieve more than 50 frames per second (FPS) up to 60 FPS. The detection threshold was configured to 0.25, which means that YOLOv5 would capture and crop the marking image only when the confidence was over 0.25.

In the first set of road trials, we tested the marking and the algorithm at different speed levels (i.e., 10, 20, 30, 40, 50 km/h) to evaluate the performance. The onboard camera (i.e., 1080p, 30 FPS) was installed with a depression angle of 23 degrees and a height of 1.57 m. In this paper, we only evaluate the performance in daylight without the help of a

heater and LED due to the lack of a high-performance thermal camera. The road trials were conducted on a sunny afternoon on a road segment of Lin Ma Hang Road, Ta Kwu Ling, New Territories, Hong Kong SAR. This road segment was a one-way, one-lane road without traffic control. The marking was placed in the middle of the traffic lane. We captured five videos at different speed levels and tested them in the laboratory afterward. Despite this, we want to emphasize that our algorithm can be run in real-time on the onboard computer.

```
video 1/1 (1034/1101) C:\Users\62746\yolov5\video\30km.MOV:
runs\detect\exp95\crops\marking\30km7.jpg
[999 0 2 999;3 7 9 2;1 6 8 4;999 1 1 999]
384x640 1 marking, Done. (0.016s)
video 1/1 (1035/1101) C:\Users\62746\yolov5\video\30km.MOV:
runs\detect\exp95\crops\marking\30km8.jpg
[999 0 2 999;3 7 9 2;1 6 8 4;999 1 1 999]
384x640 1 marking, Done. (0.016s)
video 1/1 (1036/1101) C:\Users\62746\yolov5\video\30km.MOV:
runs\detect\exp95\crops\marking\30km9.jpg
[999 0 2 999;3 7 9 2;1 6 8 4;999 1 1 999]
384x640 1 marking, Done. (0.015s)
video 1/1 (1037/1101) C:\Users\62746\yolov5\video\30km.MOV:
runs\detect\exp95\crops\marking\30km10.jpg
[999 0 2 999;3 7 9 2;1 6 8 4;999 1 1 999]
384x640 1 marking, Done. (0.015s)
```

Fig. 9. Examples of decoding results at a speed of 30 km/h.

Fig. 8 and Fig. 9 present the running output of the localization system. The marking code is presented in a list form and '999' represents the boundary markers. The average time of detecting, transformation, decoding, and filtering a frame is around 0.015 seconds, which also indicates that our algorithm can achieve more than 50 FPS on modern hardware. With the help of more advanced hardware (i.e., better CPU and GPU to accelerate the algorithm) and camera, our system can be employed at a higher FPS.

Velocity (km/h)	Number of detected frames containing markings	The correct serial number
10	18	# 8,9,10,11
20	20	# 11,12,13,15
30	11	# 7,8,9,10
40	6	# 4,5
50	5	# 3

Fig. 10. Statistic numbers of the results of road trials with a common camera.

The number of frames containing markings that are detected and cropped by YOLOv5 is illustrated in Fig. 10. It indicates that with the increase of the vehicle speed, the number of detected frames decreases. In general, our algorithm can ensure that at least five frames of the markings can be detected and captured when the speed is slower than 50 km/h. However, we can enhance the performance by adopting a high-speed camera with a higher frame rate. Additionally, in the context of the hardware, we utilized NVIDIA GeForce GTX 1650, 4096.0MB for the detection. Further study can improve the hardware to achieve a higher rate. The last column is the serial number of the correctly and completely decoded marking frame among the detected frame. All trials perform well and decode the marking correctly. The marking can be decoded 100% correctly in the first frame after half the number of frames detected. Most of the marking images can be decoded correctly in the third quartile of the detected images. When the vehicle moves slowly, around four continuous frames can be detected and decoded correctly. At least one frame can be detected and decoded correctly at a higher speed.

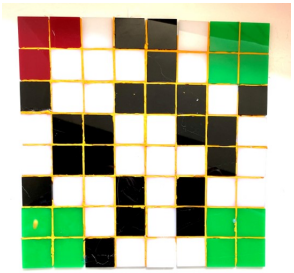

Fig. 11. Another pavement marking pattern with a randomly generated sequence of '156797763472'

Velocity (km/h)	Number of detected frames containing markings	The correct serial number
10	25	#12 to #21
20	16	#8,9,10,11,12,13,14
30	10	#5,6,7,8
40	7	# 3,4,5
50	4	# 3,4

Fig. 12. Statistic numbers of the results of road trials with another marking and a common camera.

In the first set of trials, to verify the consistency and reliability of the proposed algorithm, we made and tested another pavement marking pattern with a randomly generated sequence of '156797763472', as shown in Fig. 11. Fig. 12 presents the results from the trials, and these results are similar to the previous results provided in Fig. 10. Overall, both of these trials have similar number of detected frames when the speed is higher than 30 km/h. One more frame is decoded at 40 km/h and 50 km/h. It is apparent from this figure that more detected and decoded frames are obtained at 10 km/h and 20 km/h. The slight difference might be caused by various environmental conditions such as illumination intensity. In later trials, all the correct frames are continuously decoded, which indicates that the localization service is robust enough.

In the second set of road trials, to further test the proposed localization marking system, we conducted more trials at higher speed levels, different illumination conditions, and different shooting angles and heights. A better onboard camera (i.e., 1080p, 120 FPS) was utilized. The statistic numbers of the results of road trials are shown in Fig. 13. This first column is the serial number of the trials. The results are arranged in order of increasing speed. The third column is the specifications of the conditions of the trials. Compared with the first set of road trials, both the number of the detected frames and the number of corrected decoded frames increases

No.	Velocity (km/h)	Angles, Heights & Environmental Conditions	Number of detected frames containing markings	Number of frames correctly decoded
1	10	Depression Angle: -23°	206	182
2	20	Depression Angle: -23°	75	65
3	20	Depression Angle: -23°, Azimuth Angle: Left 15°	73	63
4	20	Depression Angle: -23°, Azimuth Angle: Right 15°	80	65
5	30	Depression Angle: -45°	57	50
6	40	Depression Angle: -23°	47	43
7	40	Depression Angle: -45°	53	46
8	50	Depression Angle: -45°	37	32
9	60	Depression Angle: -23°	29	23
10	60	Depression Angle: -23°, Height: 2.00m	31	25
11	60	Depression Angle: -45°	31	27
12	70	Depression Angle: -23°	24	21
13	70	Depression Angle: -23°, Better Illumination	30	22
14	80	Depression Angle: -23°	22	18
15	80	Depression Angle: -23°, Azimuth Angle: Right 15°	20	18
16	80	Depression Angle: -23°, Azimuth Angle: Left 15°	23	19

Fig. 13. Statistic numbers of the results of second set of road trials with a high-speed camera.

significantly due to the higher FPS. In these trials, the incorrect decoding usually happens at the end of the detection when the marking is about to leave the viewfinder so that only part of the marking can be captured. It is clear that there has been a drop in the number of correctly decoded frames with the increase in velocity. There are around 20 frames that can be detected even at the velocity of 80 km/h.

Depression angles, azimuth angles, and heights of the camera are compared via the results. Trials No.5, No.7, No.8, and No.11 were conducted with a depression angle of 45 degrees, and the others were with a depression angle of 23 degrees. The results reveal that the number of correctly decoded frames increases with the depression angle. One reason for the increased number of frames is that the deformation of the marking in the detected frame is more severe at a smaller depression angle. Even though a large expansion of scenery is established at a smaller depression angle, fewer frames are detected and decoded since the marking is so small when it is far away. However, in a bigger depression shot, the camera points down at the marking so that the marking can be detected and decoded easily once it appears in the viewfinder. Thus, more frames containing the marking are correctly decoded. Trials No.3, No.4, No.15, and No.16 were conducted with different azimuth angles. Compared with No.2 and No.14 separately, the numbers of both correctly decoded frames remain steady. Therefore, a small azimuth angle does not affect the reliability of the proposed system. Trial No.10 was conducted with a higher camera and got two more correctly decoded frames compared with No.9 due to a larger coverage of scenery.

Trial No.13 was performed in a better illuminated environment and only one more correctly decoded frame was obtained, but six more frames were detected. A better illuminated environment will help the detector identify the marking more efficiently. Overall, the most important factors that affect the performance of the algorithm are the depression angle of the camera, and the height of the camera. It can be concluded that when the marking presents in the viewfinder, the accuracy and efficiency of our system is high enough to provide a robust and accurate localization service.

IV. Conclusion

To meet the strong and increasing demand for the accurate localization service of autonomous vehicles, this paper provides a new and innovative solution. This paper firstly introduces a novel road pavement marking and provides a detailed technical description of it. Subsequently, this paper explains how to customize and train an object detector model based on YOLOv5. Then, a decoding algorithm is introduced to process the marking information and it is integrated with the YOLOv5 model so that the whole system can be run in real-time. With modern hardware, our detection and decoding algorithms can be processed with more than 50 FPS. At last, this paper conducted two sets of road trials with different cameras to examine the performance of the novel marking and associated algorithms. In the case of utilizing a normal camera, the overall results show that the marking can be decoded 100% correctly in the first frame after half of frames are detected. Most of the marking images can be decoded correctly in the third quartile of the detected images. When the vehicle moves at a speed of less than 30 km/h, at least four continuous frames can be detected and decoded correctly. When the vehicle operates at a higher speed, at least one frame can be detected and decoded correctly. In the case of utilizing a high-speed camera, more than 18 frames can be detected and decoded even at a speed of 80 km/h. This paper also investigated the effects of camera depression angles, azimuth angles, heights, and environmental conditions on the proposed localization system. The results show that the most important factor is the depression angle and the next one is the height. Overall, The findings of this paper suggest that the specially designed road marking and associated algorithms can provide a viable and economic option for the accurate localization service of autonomous vehicles.

We also reserve some features (i.e., heaters, LEDs, changeable graphic patterns, and more colors) in the marking for further enhancement and research to adjust to different working environments such as foggy days, rainy days, and nights without illumination. Moreover, the performance of the system can be further improved by employing a blur deduction algorithm and faster GPUs and CPUs.

Acknowledgment

The work was supported in part by the Research Impact Fund (Project No.R5007-18) established under the University

Grant Committee (UGC) of the Hong Kong Special Administrative Region (HKSAR), China. The work of I. W.-H. Ho was supported in part by the General Research Fund under Project 15201118, established under the University Grant Committee of the Hong Kong Special Administrative Region, China.

REFERENCES

[1] S. Kim and R. Shrestha, "Intelligent autonomous vehicle," in *Automotive Cyber Security*. Springer, 2020, pp. 15–33.

[2] K. Jo, J. Kim, D. Kim, C. Jang, and M. Sunwoo, "Development of autonomous car—part i: Distributed system architecture and development process," *IEEE Transactions on Industrial Electronics*, vol. 61, no. 12, pp. 7131–7140, 2014.

[3] S. Kuutti, S. Fallah, K. Katsaros, M. Dianati, F. Mccullough, and A. Mouzakitis, "A survey of the state-of-the-art localization techniques and their potentials for autonomous vehicle applications," *IEEE Internet of Things Journal*, vol. 5, no. 2, pp. 829–846, 2018.

[4] K. Merry and P. Bettinger, "Smartphone gps accuracy study in an urban environment," *PloS one*, vol. 14, no. 7, p. e0219890, 2019.

[5] H. Li, X. Chen, L. Huang, and D. Yao, "A gps/wi-fi integrated system for positioning in cooperative vehicle and infrastructure system," in *2012 IEEE International Conference on Vehicular Electronics and Safety (ICVES 2012)*. IEEE, 2012, pp. 285–289.

[6] H. Lu, S. Zhang, Y. Dong, and X. Lin, "A wi-fi/gps integrated system for urban vehicle positioning," in *13th International IEEE Conference on Intelligent Transportation Systems*. IEEE, 2010, pp. 1663–1668.

[7] S.-C. Yeh, W.-H. Hsu, M.-Y. Su, C.-H. Chen, and K.-H. Liu, "A study on outdoor positioning technology using gps and wifi networks," in *2009 International Conference on Networking, Sensing and Control*. IEEE, 2009, pp. 597–601.

[8] J. Zhang and Y. Zhang, "Vehicular localization based on csi-fingerprint and vector match," *IEEE Transactions on Intelligent Transportation Systems*, 2020.

[9] H. Cai, Z. Hu, G. Huang, D. Zhu, and X. Su, "Integration of gps, monocular vision, and high definition (hd) map for accurate vehicle localization," *Sensors*, vol. 18, no. 10, p. 3270, 2018.

[10] A. Y. Hata and D. F. Wolf, "Feature detection for vehicle localization in urban environments using a multilayer lidar," *IEEE Transactions on Intelligent Transportation Systems*, vol. 17, no. 2, pp. 420–429, 2015.

[11] A. Hata and D. Wolf, "Road marking detection using lidar reflective intensity data and its application to vehicle localization," in *17th International IEEE Conference on Intelligent Transportation Systems (ITSC)*. IEEE, 2014, pp. 584–589.

[12] Y. Gu, L.-T. Hsu, J. Bao, and S. Kamijo, "Integrating global navigation satellite system and road-marking detection for vehicle localization in urban traffic," *Transportation Research Record*, vol. 2595, no. 1, pp. 59–67, 2016.

[13] E. I. Adegoke, J. Zidane, E. Kampert, C. R. Ford, S. A. Birrell, and M. D. Higgins, "Infrastructure wi-fi for connected autonomous vehicle positioning: A review of the state-of-the-art," *Vehicular Communications*, vol. 20, p. 100185, 2019.

[14] T. A. Committee *et al.*, "Report on study of road traffic congestion in hong kong," *Hong Kong SAR Government: Hong Kong, China*, 2014.

[15] A. Sassani, O. Smadi, and N. Hawkins, "Developing pavement marking management systems: A theoretical model framework based on the experiences of the us transportation agencies," *Infrastructures*, vol. 6, no. 2, 2021. [Online]. Available: https://www.mdpi.com/2412-3811/6/2/18

[16] K. R. Agent, "Transverse pavement markings for speed control and accident reduction," 1980.

[17] R. A. Retting and C. M. Farmer, "Use of pavement markings to reduce excessive traffic speeds on hazardous curves," *ITE journal*, vol. 68, pp. 30–41, 1998.

[18] T. Chen, Z. Chen, Q. Shi, and X. Huang, "Road marking detection and classification using machine learning algorithms," in *2015 IEEE Intelligent Vehicles Symposium (IV)*. IEEE, 2015, pp. 617–621.

[19] T. M. Hoang, S. H. Nam, and K. R. Park, "Enhanced detection and recognition of road markings based on adaptive region of interest and deep learning," *IEEE Access*, vol. 7, pp. 109 817–109 832, 2019.

[20] S. Lee, J. Kim, J. Shin Yoon, S. Shin, O. Bailo, N. Kim, T.-H. Lee, H. Seok Hong, S.-H. Han, and I. So Kweon, "Vpgnet: Vanishing point guided network for lane and road marking detection and recognition," in *Proceedings of the IEEE international conference on computer vision*, 2017, pp. 1947–1955.

[21] P.-R. Chen, S.-Y. Lo, H.-M. Hang, S.-W. Chan, and J.-J. Lin, "Efficient road lane marking detection with deep learning," in *2018 IEEE 23rd International Conference on Digital Signal Processing (DSP)*. IEEE, 2018, pp. 1–5.

[22] J. Hu, S. Abubakar, S. Liu, X. Dai, G. Yang, and H. Sha, "Near-infrared road-marking detection based on a modified faster regional convolutional neural network," *Journal of Sensors*, vol. 2019, 2019.

[23] D. Gruyer, R. Belaroussi, and M. Revilloud, "Accurate lateral positioning from map data and road marking detection," *Expert Systems with Applications*, vol. 43, pp. 1–8, 2016.

[24] T. Wu and A. Ranganathan, "Vehicle localization using road markings," in *2013 IEEE Intelligent Vehicles Symposium (IV)*. IEEE, 2013, pp. 1185–1190.

[25] J. Jeong, Y. Cho, and A. Kim, "Road-slam: Road marking based slam with lane-level accuracy," in *2017 IEEE Intelligent Vehicles Symposium (IV)*. IEEE, 2017, pp. 1736–1473.

[26] Q. Tao, Z. Hu, H. Cai, G. Huang, and J. Wu, "Coding pavement lanes for accurate self-localization of intelligent vehicles," in *2018 IEEE Intelligent Vehicles Symposium (IV)*. IEEE, 2018, pp. 1458–1463.

[27] J. Du and M. J. Barth, "Next-generation automated vehicle location systems: Positioning at the lane level," *IEEE Transactions on Intelligent Transportation Systems*, vol. 9, no. 1, pp. 48–57, 2008.

[28] H. Hu, D. Vizzari, X. Zha, and R. Roberts, "Solar pavements: A critical review," *Renewable and Sustainable Energy Reviews*, vol. 152, p. 111712, 2021.

[29] N. Dalal and B. Triggs, "Histograms of oriented gradients for human detection," in *2005 IEEE computer society conference on computer vision and pattern recognition (CVPR'05)*, vol. 1. Ieee, 2005, pp. 886–893.

[30] F. Zhou, H. Zhao, and Z. Nie, "Safety helmet detection based on yolov5," in *2021 IEEE International Conference on Power Electronics, Computer Applications (ICPECA)*. IEEE, 2021, pp. 6–11.

[31] J. Redmon, S. Divvala, R. Girshick, and A. Farhadi, "You only look once: Unified, real-time object detection," in *Proceedings of the IEEE conference on computer vision and pattern recognition*, 2016, pp. 779–788.

[32] G. Jocher, A. Stoken, J. Borovec, NanoCode012, ChristopherSTAN, L. Changyu, Laughing, tkianai, A. Hogan, lorenzomammana, yxNONG, AlexWang1900, L. Diaconu, Marc, wanghaoyang0106, ml5ah, Doug, F. Ingham, Frederik, Guilhen, Hatovix, J. Poznanski, J. Fang, L. Yu, changyu98, M. Wang, N. Gupta, O. Akhtar, PetrDvoracek, and P. Rai, "ultralytics/yolov5: v3.1 - Bug Fixes and Performance Improvements," Oct. 2020. [Online]. Available: https://doi.org/10.5281/zenodo.4154370

[33] R. Xu, H. Lin, K. Lu, L. Cao, and Y. Liu, "A forest fire detection system based on ensemble learning," *Forests*, vol. 12, no. 2, p. 217, 2021.

[34] U. Nepal and H. Eslamiat, "Comparing yolov3, yolov4 and yolov5 for autonomous landing spot detection in faulty uavs," *Sensors*, vol. 22, no. 2, p. 464, 2022.

Yuhao Wang was born in Shuangyashan, Heilongjiang, China. He received the B.Eng. degree in traffic engineering from Southeast University, China, in 2018 and the M.S. degree in transport from Imperial College London in 2019. He is currently working toward the Ph.D. degree with The Hong Kong Polytechnic University, Kowloon, Hong Kong, focusing on intelligent transport system and smart pavement. His work on a smart, integrated road pavement and drainage system for storm-water storage, deicing, dust suppression, and cooling received the Gold Medal with the Organizer's Choice Award in the International Invention Innovation Competition in Canada (iCAN) in 2020.

Yuhong Wang received his M.Eng. and B.Eng. degree at Tongji University, Shanghai, China in 1996, and the Ph.D. and MSc in civil engineering at the University of Kentucky, the USA in 2003 and 2001, respectively. He is currently a Professor with the Department of Civil and Environmental Engineering, Hong Kong Polytechnic University, Hong Kong. His research interest focuses on the new generation of urban infrastructure, which includes how to make future cities cleaner and more environmentally friendly, more resistant to floods, better serve urban residents, smarter, and how to promote biodiversity in the urban environment.

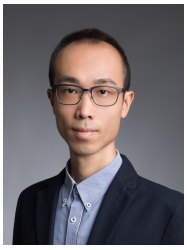

Ivan Wang-Hei Ho (M'10–SM'18) received the B.Eng. and M.Phil. degrees in information engineering from The Chinese University of Hong Kong, Hong Kong, in 2004 and 2006, respectively, and the Ph.D. degree in electrical and electronic engineering from the Imperial College London, London, U.K., in 2010. He was a Research Intern with the IBM Thomas J. Watson Research Center, Hawthorne, NY, USA, and a Postdoctoral Research Associate with the System Engineering Initiative, Imperial College London. In 2010, he cofounded P2 Mobile Technologies Ltd., where he was the Chief Research and Development Engineer. He is currently an Associate Professor with the Department of Electronic and Information Engineering, The Hong Kong Polytechnic University, Hong Kong. His research interests include wireless communications and networking, specifically in vehicular networks, intelligent transportation systems (ITS), and Internet of things (IoT). He primarily invented the MeshRanger series wireless mesh embedded system, which received the Silver Award in Best Ubiquitous Networking at the Hong Kong ICT Awards 2012. His work on indoor positioning and IoT also received a number of awards, including the Gold Medal at the International Trade Fair Ideas and Inventions New Products (iENA) in 2019, the Gold Medal with the Organizer's Choice Award at the International Invention Innovation Competition in Canada (iCAN) in 2020, and the Gold Medal at the International Exhibition of Inventions Geneva in 2021. He is currently an Associate Editor for the IEEE Access and IEEE Transactions on Circuit and Systems II.

Wei Sheng is a Ph.D. candidate from The Hong Kong Polytechnic University. Prof. Yuhong Wang is his supervisor. The "Smart Pavements" project support him to complete his Ph.D. degree. His research topic is mainly focus on functions and durabilty of prefabricated conrete pavement textures. such textures are produced with the assistance of 3D printing technology. In addition, He is also involved in other research topics, including texture-induced drainage system, accurate positioning device for autonomous driving technology, etc.

Ling Chen received her bachelor and master degree in Sun Yat-Sen University (Guangzhou). Then, she worked as a research assistant in the Hong Kong polytechnic university and received her Ph.D. degree in the Hong Kong polytechnic university. Currently, she is a lecturer at Xidian University. Her research interests are image processing, machine learning, and data science methods involved in engineering fields.